Analysis on Characteristics of Structural Impact Response of Airborne Armored Vehicle in Landing Process

IOP Conf. Series: Materials Science and Engineering **484** (2019) 012024 doi:10.1088/1757-899X/484/1/012024

Analysis on Characteristics of Structural Impact Response of Airborne Armored Vehicle in Landing Process

Xinhua Fu

Airborne Training Center, Guilin, Guangxi, 541003, China
E-mail: fuxinhua_003@163.com

Abstract. For such problems as high cost and complex implementation in analyzing the characteristics of the structural impact response of airborne armored vehicle in landing process by real equipment airdrop test, finite element method(FEM) was taken to build the finite element(FE) model of airborne armored vehicle and airbag system to simulate the landing impact process of airborne armored vehicle and that under different typical airdrop conditions of airborne armored vehicle, including different altitude and different vertical landing speed. In addition, comprehensive quantitative analysis was conducted on the characteristics of the structural impact response of airborne armored vehicle to provide theoretical guidance for the design, development, operational use and maintenance of airborne armored vehicle.

1. Introduction

The impact load in the landing process of airborne armored vehicle is one of the major factors causing vehicle structure damage. The structural dynamic response in the landing buffering process of airborne armored vehicle is an important characteristic and is an important indicator to evaluate the stiffness and strength of equipment structure. Real equipment airdrop test and numerical simulation are currently the most common methods to analyze the characteristics of structural impact response of airborne armored vehicle under landing impact conditions. The landing conditions of airborne armored vehicle vary in a large range and are difficult to predict due to the influence of climate and ground environmental conditions. The implementation of the real equipment airdrop test under multiple conditions needs enormous human, material and financial resources. At the beginning of the development and approval test of airborne armored vehicle, the real equipment airdrop test was conducted on airborne armored vehicle. However, limited test data were insufficient to study structural impact response characteristics [1-2]. The development of computer technology and finite element theory has provided a new method for studying the characteristics of structural impact response of airborne armored vehicle in landing process in recent years. FEM was taken in this paper to build the FE model of airborne armored vehicle and airbag system to simulate the landing impact process of airborne armored vehicle and analyze structural impact response characteristics so as to provide theoretical guidance for the design, development, operational use and maintenance of airborne armored vehicle.

2. Analysis Process and Build of Finite Element Analysis (FEA) Model

2.1. Analysis Process

The analysis process of the characteristics of structural impact response is as shown in Fig. 1. The whole analysis process is based on Ansys Workbench, LS-DYNA, Mechanical and so on. First of all, the FE model of airborne armored vehicle and airbag system is built by such steps as geometric model

building, material definition, meshing, setting contact relationship, setting initial conditions, setting constraints, solution setup, outputting K files and editing and modifying K files. Next, the landing buffering process under typical airdrop conditions (including different altitude and different vertical landing speed) of airborne armored vehicle was simulated on the basis of the FE model of airborne armored vehicle and airbag system built to obtain such simulation results as stress distribution cloud map, stress change curve and plastic strain field cloud map and conduct comprehensive quantitative analysis on the characteristics of the structural impact response of airborne armored vehicle.

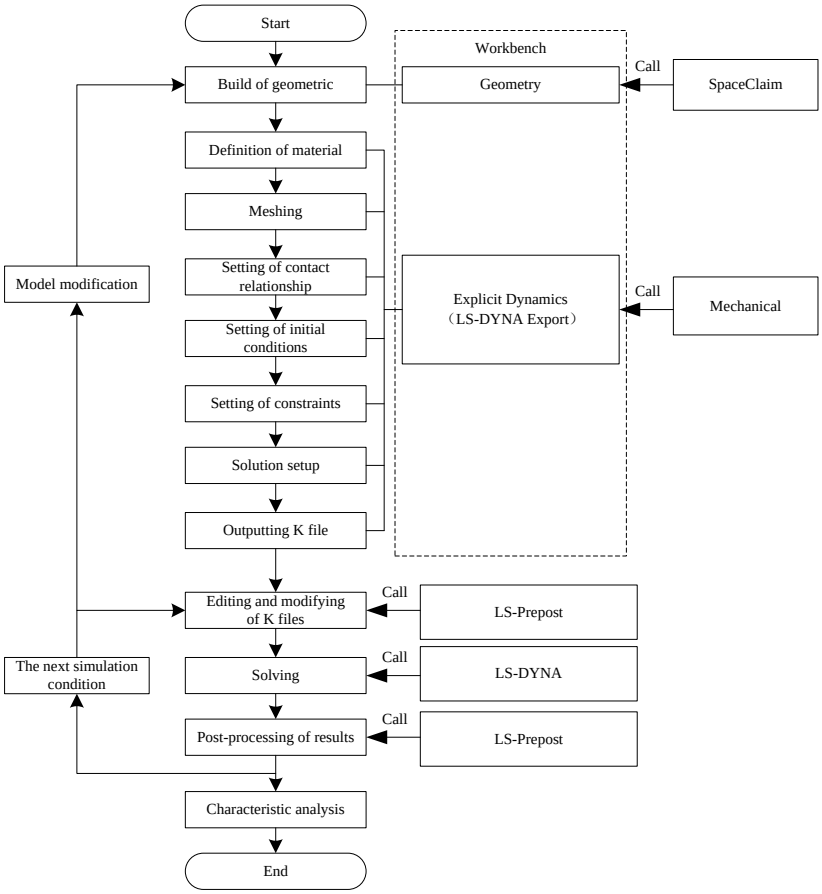

Figure 1. Analysis Process of Characteristics of Structural Impact Response

2.2. FE Model of Airborne Armored Vehicle and Airbag System

In order to improve the efficiency of simulation, when building the FE model of the vehicle body, the structure is necessarily simplified by omitting non-load-bearing components, removing tiny structural characteristics, smoothing the surface of the components and configuring the non-load-bearing components with large mass in the form of mass points on the premise of ensuring the accuracy of calculation [1]. Since the armor plate of the vehicle body of airborne armored vehicle is thin, it is meshed by shell element. Some solid structures, such as turret base ring and support, are meshed by body element. The main body support structure, engine support and other components are identified as the weak parts of the vehicle body structure according to the results of preliminary simulation. Therefore, mesh refinement is conducted on such components.

The buffering airbag system of the airborne armored vehicle is composed of 8 independent airbags in parallel. Since only the landing buffering process is studied, the folding of airbag before landing process and the unfolding of airbag during landing process are not considered. Therefore, the airbag model is in an unfolded state. The airbag is meshed by shell element. Control volume method is taken to establish buffering airbag model on the basis of ideal gas homogeneous pressure model.

The airbag will generate significant compression deformation in the landing buffering process. Both the self-contact model of airbag and the contact model of the airbag with the ground, the vehicle body and the airbag plate are solved by penalty function. The FE model of airborne armored vehicle and airbag system built is as shown in Fig. 2.

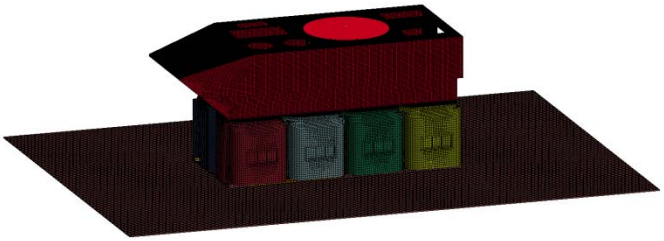

Figure 2. FE model of airborne armored vehicle and airbag system

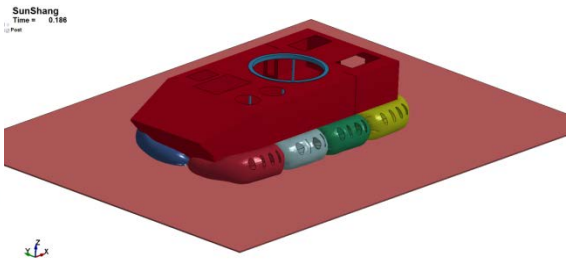

Figure 3. Landing buffering state of vehicle at V=8m/s and the max stress

2.3. Constitutive Material Model

Johnson-Cook model is used to construct the constitutive relations of structural materials of airborne armored vehicle. Johnson-Cook model can reflect the effects of strain hardening, strain rate hardening and temperature softening. Its flow stress-plastic strain expression is [3]:

$$\sigma = \left(A + B\bar{\varepsilon}^{p^n}\right)\left(1 + C\ln\dot{\varepsilon}^*\right)\left(1 - T^{*m}\right)$$

Where, σ is flow stress; *A, B, n, C and m* are constitutive parameters: *A* is yield strength of material, *B* is hardening modulus, *n* is plasticity hardening index, and *C* is strain rate coefficient; $\bar{\varepsilon}^p$ is equivalent plastic strain; and $\dot{\varepsilon}^*$ is dimensionless strain rate.

$\dot{\varepsilon}^* = \frac{\dot{\bar{\varepsilon}}^p}{\dot{\varepsilon}_0}$, $\dot{\bar{\varepsilon}}^p$ is actual strain rate, $\dot{\varepsilon}_0$ is reference strain rate which usually is $1s^{-1}$.

$T^* = \frac{T - T_{room}}{T_{melt} - T_{room}}$, T is material temperature (test temperature), T_{room} is reference temperature which usually is the ambient temperature, and T_{melt} is the melting temperature of material.

3. Simulation of Characteristics of Structural Impact Response

3.1. Simulation Results

The landing buffering process under typical airdrop conditions of airborne armored vehicle was simulated. The structural impact response of vehicle at different vertical landing speed in plain area (the altitude is approximately 0m) is as shown in Table 1 and that upon landing at different altitude as shown in Table 2. The italic numbers in the table means that the element number corresponding to the max stress value of certain part is different from that corresponding to the max plastic strain.

Table 1. Structural Impact Response of Vehicle at Different Vertical Landing Speed (Plain Area)

Vertical landing speed (m/s)	Typical part	Specific element number	Max stress value (MPa)	Max plastic stress (%)
V=8	Armor plate	361583	216.88	0
	Front left column bottom	202515	304.95	0
	Front right column bottom	202183	348.21	0
	Back left column bottom	201906	320.58	0
	Back right column bottom	202330	361.42	0
	Bottom of engine back support	265729	137.14	0
	Bottom of engine front left support	265730	185.02	0
	Bottom of engine front right support	268979	177.47	0
V=9	Armor plate	320806	487.50	0.46
	Front left column bottom	143924	513.52	1.50
	Front right column bottom	202183	518.64	0.92
	Back left column bottom	201906	522.67	0.97
	Back right column bottom	202330	525.42	1.01
	Bottom of engine back support	265729	459.91	0.06
	Bottom of engine front left support	265730	497.84	0.61
	Bottom of engine front right support	268979	513.66	1.43
V=10	Armor plate	288854	***559.34***	2.40
		289279	532.10	***2.58***
	Front left column bottom	143962	865.41	6.68
	Front right column bottom	137082	738.75	4.50
	Back left column bottom	137731	***910.83***	7.47
		137730	910.32	***7.54***
	Back right column bottom	150185	701.82	3.94
	Bottom of engine back support	265729	514.47	1.65
	Bottom of engine front left support	265730	***528.66***	1.14
		265734	512.80	***1.34***
	Bottom of engine front right support	268979	702.03	6.55

Table 2. Structural Impact Response of Vehicle at Different Landing Ground Altitude (V=8m/s)

Landing Ground Altitude (m)	Typical part	Specific element number	Max stress value (MPa)	Max plastic stress (%)
H=1000	Armor plate	361583	***436.30***	0.00
		289279	326.74	***0.05***
	Front left column bottom	202515	469.59	0.19
	Front right column bottom	202183	482.62	0.38
	Back left column bottom	201906	475.42	0.27
	Back right column bottom	202330	481.11	0.36
	Bottom of engine back support	265729	428.13	0.00
	Bottom of engine front left support	265730	459.27	0.03
	Bottom of engine front right support	268979	458.49	0.05

Table 3. Structural Impact Response of Vehicle at Different Landing Ground Altitude (V=8m/s)(Cont.)

Landing Ground Altitude (m)	Typical part	Specific element number	Max stress value (MPa)	Max plastic stress (%)
H=2000	Armor plate	320806	***490.04***	0.50
		289279	454.79	***0.75***
	Front left column bottom	143924	596.74	3.95
	Front right column bottom	202183	538.22	1.23
	Back left column bottom	201906	553.54	1.69
	Back right column bottom	202330	542.64	1.27
	Bottom of engine back support	265729	458.61	0.02
	Bottom of engine front left support	265730	499.78	0.64
	Bottom of engine front right support	268979	536.59	1.79
H=3000	Armor plate	288854	***501.79***	1.30
		289279	497.92	***1.74***
	Front left column bottom	143962	727.91	5.52
	Front right column bottom	202183	573.35	2.11
	Back left column bottom	137731	750.00	5.36
	Back right column bottom	202330	588.90	2.21
	Bottom of engine back support	263659	***458.95***	0.02
		265725	458.29	***0.04***
	Bottom of engine front left support	267234	514.54	0.88
	Bottom of engine front right support	268979	593.50	3.56
H=4000	Armor plate	288854	658.66	4.12
	Front left column bottom	143962	901.88	7.75
	Front right column bottom	137082	743.91	4.54
	Back left column bottom	137731	945.54	8.82
	Back right column bottom	150185	764.22	4.66
	Bottom of engine back support	265729	515.85	1.80
	Bottom of engine front left support	265734	548.46	2.45
	Bottom of engine front right support	268979	764.44	8.46

3.2. Result Analysis

(1) Without loss of generality, characteristic analysis is conducted on the basis of the structural impact response of airborne armored vehicle in plain area and at vertical landing speed of V=8m/s.

1) As shown in Fig. 3, in the landing buffering process of airborne armored vehicle, at 0.186s, the armor plate of airborne armored vehicle contacts the ground (closest to the ground), the vehicle body structure undergoes the max impact overload and the whole vehicle generates the max stress.

2) The max von Mises stress distribution cloud map of the whole vehicle is as shown in Fig. 4. The max comprehensive stress is located at the root of the bottom of the back right column of the main support of the vehicle body, and the max stress is 361.42MPa. The stress of the whole vehicle is mainly distributed on the frame, especially at the bottom of the 4 columns of the fighting cabin and on the girder of the bottom armor plate. The stress on the vehicle armor plate is significantly smaller than that on the main support, indicating that the frame has played a very good enhancement function to the vehicle body structure and has absorbed most of the impact energy. In the landing process of the airborne armored vehicle, the time and position of generation of the max stress, the max first principal stress and the max shear stress may be different.

3) The stress change curve at the max stress position is as shown in Fig. 5. The generation time of the max stress of each component/part of the vehicle is different during landing buffering. Before the bottom armor plate of vehicle contacts the ground, the stress at all positions of vehicle body gets greater with the buffering process and increases quickly to the max value in the moment of contacting the ground, after which the stress oscillates at a low frequency. The stress oscillation frequency and amplitude of body components at different positions are different.

4) When the airborne armored vehicle is under the effect of normal landing process impact, i.e. the airborne armored vehicle realizes landing process in plain area at a vertical landing speed below 8m/s, according to the first and fourth strength theory of material mechanics, since the structural stress of the vehicle body does not exceed the yield limit of the material, the vehicle body will not produce plastic strain, indicating that the strength of the vehicle body meets airdrop requirements.

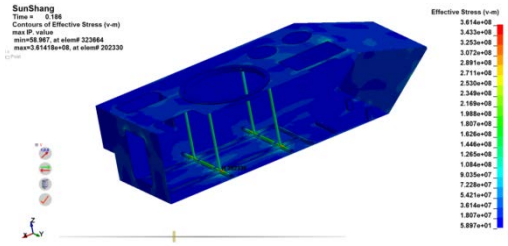

Figure 4. The max von Mises stress distribution cloud map at V=8m/s

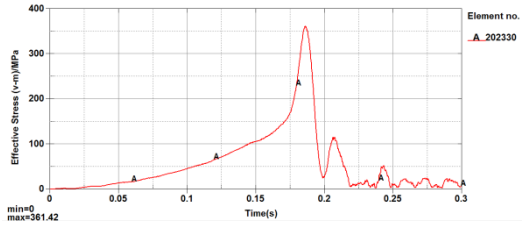

Figure 5. Stress change curve at the max stress position at V=8m/s

(2) When the vertical landing speed of vehicle V=9m/s, the vehicle body structure shows plastic strain, indicating that landing impact overload on the vehicle body structure increases with the increase of the vertical landing speed. Besides, the structural stress of the vehicle body increases accordingly and exceeds the yield limit of the material. The vehicle body structure shows deformation. When the vertical landing speed of vehicle V=10m/s, the vehicle body structure shows great plastic strain (as shown in Fig. 6) which is almost close to the plastic strain corresponding to the damage threshold of the material, indicating that the ultimate vertical landing speed of the airborne armored vehicle allowed by single airdrop in plain area is 10m/s.

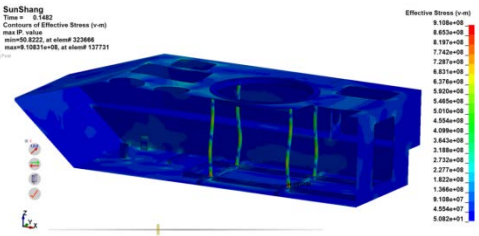

Figure 6. The max von Mises stress distribution cloud map at V=10m/s

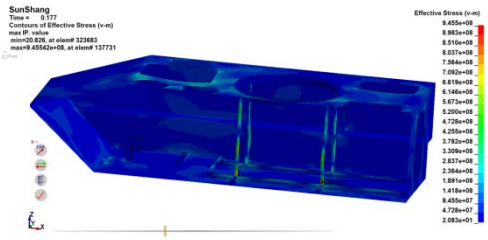

Figure 7. The max von Mises stress distribution cloud map at H=4,000m

(3) Under different vertical landing speed, i.e. under different airdrop conditions, the time and position of the max stress of the vehicle body structure may be different, and the position of the max stress value may be different from the max plastic strain. The oscillation frequency and amplitude of the stress change curve at the max stress position increase with the increase of the vertical landing speed.

(4) When the landing ground altitude H=0m, the vehicle body structure shows no plastic strain. When the landing ground altitude H=1000m, the vehicle body structure shows plastic strain, indicating that landing impact overload on the vehicle body structure increases with the increase of the landing ground altitude. Besides, the structural stress of the vehicle body increases accordingly and exceeds the yield limit of the material. The vehicle body structure shows deformation.

(5) With the gradual increase of landing ground altitude, the max stress and the max plastic strain also increase gradually. When the landing ground altitude H=4,000m, the vehicle body structure shows great plastic strain. That at some positions has exceeded the plastic strain corresponding to the damage threshold of the material (as shown in Fig. 7), indicating that the airborne armored vehicle can realize landing process only in areas below the altitude of 4,000m when the vertical landing speed is 8m/s. If the landing ground altitude is higher than this altitude, the airborne armored vehicle will have

more serious damage and exceed the damage threshold of the material, making the mission unsuccessful.

(6) Under different landing ground altitude, i.e. under different landing process conditions, the time and position of the max stress of the vehicle body structure may be different; and the position of the max stress value may also be different from the max plastic strain. The oscillation frequency and amplitude of the stress change curve at the max stress position increase with the increase of the landing ground altitude.

4. Conclusions

FEM was applied to build the FE model of airborne armored vehicle and airbag system to simulate the landing impact process of airborne armored vehicle, analyze its structural impact response characteristics and simulate the landing impact process under typical airdrop conditions of airborne armored vehicle. The following conclusions are drawn: 1) when the airborne armored vehicle realizes landing process in plain area at a vertical landing speed below 8m/s, since the structural stress of the vehicle body does not exceed the yield limit of the material, the vehicle body will not have plastic strain and the strength of the vehicle body meets airdrop requirements; 2) in order to ensure safe airdrop of the airborne armored vehicle, the ultimate vertical landing speed of the airborne armored vehicle allowed by single airdrop in plain area is 10m/s. When the vertical landing speed is 8m/s, the airborne armored vehicle can land only in areas below the altitude of 4,000m.

5. References

[1] LI Jian-yang, WANG Hong-yan, RUI Qiang , HONG Huang-jie , ZHANG Fang. Research on Cumulative Damage Assessment Method for Airborne Vehicle at Landing Based on Finite Element Analysis [J]. Journal of System Simulation, 2014.1, 26(1): 208-214.

[2] LI Jian-yang, WANG Hong-yan, HAO Gui-xiang. Simulation of Landing Process Based on Explicit Finite Element Method [J]. Journal of Academy of Armored Force Engineering, 2010.6, 24(3): 25-28.

[3] LI Yun-fei, ZENG Xiang-guo, LIAO Yi. Thermal-viscoplastic constitutive relation of Ti-6A1-4V alloy and numerical simulation by modified Johnson-Cook modal [J]. The Chinese Journal of Nonferrous Metals, 2017.7, 27(7): 1419-1425.